

Catalysis Science & Technology

Accepted Manuscript



This is an *Accepted Manuscript*, which has been through the Royal Society of Chemistry peer review process and has been accepted for publication.

Accepted Manuscripts are published online shortly after acceptance, before technical editing, formatting and proof reading. Using this free service, authors can make their results available to the community, in citable form, before we publish the edited article. We will replace this *Accepted Manuscript* with the edited and formatted *Advance Article* as soon as it is available.

You can find more information about *Accepted Manuscripts* in the [Information for Authors](#).

Please note that technical editing may introduce minor changes to the text and/or graphics, which may alter content. The journal's standard [Terms & Conditions](#) and the [Ethical guidelines](#) still apply. In no event shall the Royal Society of Chemistry be held responsible for any errors or omissions in this *Accepted Manuscript* or any consequences arising from the use of any information it contains.

Attrition-Resistant Ni-Mg/Al₂O₃ Catalyst for Fluidized Bed Syngas Methanation

Dianmiao Cui^{1,2}, Jiao Liu¹, Jian Yu¹, Fabing Su¹, Guangwen Xu^{1*}

* Corresponding author. Tel./Fax: +86-10-8254-4429, E-mail address: gw Xu@ipe.ac.cn

¹ State Key Laboratory of Multi-phase Complex Systems, Institute of Process Engineering, Chinese Academy of Sciences, Beijing 100190, China

² University of Chinese Academy of Sciences, Beijing 100049, China

Abstract: Spray granulation was applied to prepare attrition-resistant Ni-Mg/Al₂O₃ catalysts for fluidized bed methanation. The tested binders included alumina sol (AS, pH = 4.0), acidic silica sol (SS, pH = 3.0), alumina-modified silica sol (AM, pH = 8.7) and alkaline silica sol (CC, pH = 9.6). By air-jet attrition test it was found that the attrition strength of the resulting catalysts followed an order of C-SS > C-AM > C-AS > C-CC, here C-SS, as an example, refers to the catalyst using SS as the binder. Characterization shows that the higher volume of pores above 20 nm, the less attrition resistance of the catalyst was, especially for the catalysts using silica binders whose high particle density was also beneficial to improving the attrition resistance of the catalyst. Syngas methanation over the catalysts in a fluidized bed at 2.5 MPa clarified an activity order of C-AS > C-SS > C-AM ≈ C-CC at 623-923 K. The AS binder enabled highly dispersed metallic Ni and many surface active sites for methanation reactions. Continuous methanation for 20 h at 900 K and 2.5 MPa verified the stability of the catalysts using the AS, SS and CC binders, but the activity obviously decreased over C-AM. Analyzing the spent catalysts via TPO demonstrated a high amount of inactive carbon on C-AM to cause its deactivation in the 20-h test.

Keywords: Methanation; SNG; Fluidized bed; Spray granulation; Attrition

1. Introduction

Methanation of syngas for the production of substitute natural gas (SNG) is currently attracting great attention, especially in China, because of its anticipated effective use of the coal resource in remote areas and the supplementary guarantee of the nation's gaseous energy supply. Syngas methanation is highly exothermic ($\text{CO} + \text{H}_2 \rightarrow \text{CH}_4 + \text{H}_2\text{O}$, $\Delta H_{298\text{K}} = -206.1 \text{ kJ}\cdot\text{mol}^{-1}$) and the major challenge in developing the technology is to remove the reaction heat and maintain the reaction temperature. Since the 1970s, a number of methanation technologies have been developed by using fixed and fluidized bed reactors.¹ The adiabatic fixed bed methanation technology usually consists of several reactors in series with intermediate gas cooling units and product gas recycling lines. The process itself is complicated and relatively difficult to control, where it is highly possible to occur sintering of catalysts in fixed bed due to the locally high reaction temperatures.¹ The fluidized bed reactors can be operated under isothermal conditions, and it is well known to be suitable for handling highly exothermic reactions at high capacities.² A few studies on fluidized bed methanation have been well done at the laboratory and pilot scales,³⁻⁶ and its superiority in terms of higher CO conversion and less carbon deposition over fixed bed methanation was well confirmed.⁶ However, special effort is required to overcome the attrition of catalyst in fluidized bed reactors. High mechanical strength is expected for reducing the loss of expensive catalyst and also avoiding the unstable fluidization due to the attrition-induced decrease in particle sizes.^{7,8} Up to now, no attrition-resistant methanation catalyst has been reported.

Impregnation on support material and adding binder additives are the effective ways to prepare catalysts for fluidized bed. The impregnated catalysts can improve catalyst attrition resistance but at the expense of low specific activity.⁹ Meanwhile, impregnation is not suitable for catalysts asking high metal loading.⁹⁻¹¹ Binder, as hard and relatively inert material, is widely used to embed small particles of active catalyst in a rigid continuous framework or skeleton to impart the formed particles attrition resistance.^{12, 13} Bukur et al.¹⁴ found that iron-base F-T catalysts using silica as the binder at intermediate SiO₂ contents (10-12 wt%) had the expected high attrition resistance. Bergna¹³ prepared attrition-resistant porous particles by mixing micron-size particles and discrete nanoparticles of silica binder. In addition, alumina-sol, kaolin and pseudo-boehmite are all widely used as binding materials in the preparation of commercial FCC catalysts.

Apart from the attrition resistance, the other physical properties such as spherical shape, appropriate particle size and packing density are also entailed for the catalysts used in fluidized bed reactors. Spray granulation can achieve the basic requirements for making particles with spherical shape, uniform sizes and packing density, and it has been widely applied in the preparation of fluid catalytic cracking (FCC) catalysts, iron F-T catalysts, fluidized bed acrylonitrile catalysts, and so on.^{12, 15, 16} For syngas methanation catalyst, the active component, say NiO species, has to be well dispersed on the support to supply the sufficiently high catalytic activity but moderate interactions with the support to avoid catalyst deactivation due to nickel sintering and carbon deposition.¹⁷⁻²⁰ Thus, the difficulty for making the fluidized bed methanation

catalyst is how to bind the active component and the support into a hard framework to improve the attrition resistance but without much sacrifice of the activity and selectivity of the catalyst.

In this study we prepared four Ni-Mg/Al₂O₃ fluidized bed methanation catalysts via spray granulation using silica-sol and alumina-sol as the binder to bind the catalyst precursor particles. The goal is to study the effect of two binder systems on attrition resistance and catalytic activity of the precipitated nickel-base catalyst. Meanwhile, the study also investigated the relationship between the catalyst attrition resistance and the structure and particle properties of the catalysts in the calcined state. These studies are expected to optimize the type of binder material for preparing the attrition-resistant methanation catalyst suitable for fluidized bed reactors.

2. Experimental

2.1 Catalyst preparation

All chemicals had the technical grade and were used without further purifications. Catalysts were prepared in this work at scales of kilograms through following two basic steps: (1) preparation of Ni-Mg/Al₂O₃ precursor and (2) incorporation of silica or alumina binder for spray granulation. The Ni-Mg/Al₂O₃ precursor was prepared via acid-base pairing method coupling hydrothermal treatment. Aqueous solutions of NaAlO₂ and metal nitrates including Ni(NO₃)₂·6H₂O, Mg(NO₃)₂·6H₂O and Al(NO₃)₃·9H₂O were first added dropwise into a vessel kept at 338 K under continuous mechanical stirring. The addition rate of the solutions and the ratio of Al(NO₃)₃·9H₂O to NaAlO₂ were controlled to maintain the reaction mixture for pH =

11. After coprecipitation the solution was subjected to a pressurized hydrothermal treatment at 473 K for 10 h, and the resulting precipitate was, in succession, aged, washed, filtered and dried at 393 K for 10 h to obtain the precursor.

In turn, the precursor was crushed into powder smaller than 5 μm and slurried with a certain amount of binder, either silica or alumina sol. In this study, three kinds of silica sols, acidic silica sol (SS, pH = 3.0), alumina-modified silica sol (AM, pH = 8.7) and alkaline silica sol (CC, pH = 9.6), and one alumina sol (AS, pH = 4.0) with similar particle sizes of 9 - 20 nm were used as binders. Spray granulation in a bench-scale spray dryer was performed to make spherical particles with relatively uniform size distribution. The catalyst was finally obtained by calcination at 873 K for 4 h in a muffle furnace. The obtained catalysts prepared with different binders were designated as C-AS, C-SS, C-AM and C-CC according to their different binders used. Another catalyst with the weight composition of 20Ni/10Mg/70Al₂O₃ (denoted as 20Ni) but without binder was prepared following the first step described above as a benchmark. The NiO contents of all prepared catalysts are listed in Table 1, showing that all are about 22 wt%.

2.2 Catalyst characterization

The attrition resistance of the catalysts made by spray granulation was evaluated in their calcined states by the modified air-jet attrition test, an ASTM method widely employed to measure the attrition of FCC catalyst. According to the air-jet test, 35 g sample of 40 - 125 μm was entrained with an air flow of 9 L·min⁻¹ (relative humidity being 35 \pm 5%) for 5 h. After test, the catalysts below 40 μm remaining in the attrition

tube and that collected by a thimble filter at the outlet of the settling chamber were defined as fines. The attrition index (*AI*) is defined as follows:

$$AI (\%) = [\text{total fine collected in 5 h (g)}/\text{initial sample amount (35g)}]/5 \times 100\%.$$

A lower *AI* indicates the better attrition resistance of the sprayed catalysts. In this work, a commercial $\gamma\text{-Al}_2\text{O}_3$ powder widely used as the support of fluidized bed catalysts was employed as a comparison standard.

The particle size distribution (PSD) of the catalyst was measured using a laser particle size analyzer (Mastersizer 2000, Malvern). Particle morphology was observed for each catalyst using a field emission scanning electron microscope (SEM; JSM-7001F, JEOL). The microscopic feature of the catalyst was obtained by the transmission electron microscopy (TEM; JEM-2010F, JEOL) that has an accelerating voltage of 200 kV. Nitrogen adsorption-desorption isotherms of the catalysts were measured at 77 K via physisorption analyzer (ASAP 2020, Micromeritics). The pore size distribution was calculated with the Barrett-Joyner-Hallender (BJH) method applied to the desorption branch, and the specific surface area was calculated according to the Brunauer-Emmett-Teller (BET) method in the relative pressure (p/p_0) range of 0.06-0.15. Prior to measurement, each sample was thoroughly degassed at 373 K for 1 h and then at 573 K for 4 h. High-pressure mercury displacement (AutoPore IV 9510, Micromeritics) and N_2 physisorption pore-volume measurements (AccuPyc 1340, Micromeritics) were used to determine the particle and skeletal densities of a catalyst. The crystal structure of a catalyst was analyzed using X-ray powder diffractometer (XRD; X'Pert PRO MPD, PANalytical) with the Cu $K\alpha$

radiation ($\lambda=1.5418 \text{ \AA}$).

The temperature-programmed reduction (TPR), temperature-programmed oxidation (TPO) and H_2 chemisorption measurement were carried out using an automated chemisorption analyzer (chemBET pulsar TPR/TPD, Quantachrome). A sample of 50 mg was loaded into a quartz U-tube reactor and dried at 373 K for 60 min in a helium stream. The H_2 -TPR test was performed by heating the sample to 1273 K at $5 \text{ K}\cdot\text{min}^{-1}$ in an Ar-base gas containing 10 vol% H_2 , and the consumed H_2 in the process was monitored with a process mass spectrometry (Proline MS, AMETEK). For testing TPO, after pretreatment at 373 K for 60 min in a helium flow, 50 mg of the spent catalyst was heated to 1273 K at $5 \text{ K}\cdot\text{min}^{-1}$ in a N_2 -base gas containing 10 vol% O_2 . The emitted CO_2 was also monitored on-line with the MS. For H_2 uptake, catalyst was firstly reduced in a flow of hydrogen at 1073 K for 4 h. Then the sample was flushed in a pure Ar (99.99%) gas flow for an hour and cooled down to 323 K. Hydrogen (30 mL) was injected in pulse to the reduced catalyst until no H_2 -adsorption could be detected. The nickel surface area was calculated by assuming a stoichiometry ratio of $\text{H}/\text{Ni} = 1$ on the catalyst surface.²¹

2.3 Activity and attrition evaluations

For evaluating catalyst activity, 2.5 g catalyst of 40-125 μm was loaded into a stainless steel fluidized bed reactor (30 mm in i.d.) and the methanation was at 623-923 K, 2.5 MPa and a space velocity (SV) of $120 \text{ NL}\cdot\text{g}^{-1}\cdot\text{h}^{-1}$. Stability test was carried out in a stainless steel fixed bed reactor (30 mm in i.d.) at 900 K and 2.5 MPa using 1.5 g catalyst under a space velocity (SV) of $200 \text{ NL}\cdot\text{g}^{-1}\cdot\text{h}^{-1}$. A gas mixture

containing H₂, CO and N₂ made according to H₂/CO/N₂ = 3/1/1 (in molar ratio) was adopted as the feeding gas. In prior to reaction the catalyst was reduced via a temperature programme from room temperature to 1273 K at 5 K·min⁻¹ and atmospheric pressure in a N₂-base gas containing 10 vol% H₂. The effluent gas from the reactor was cooled in an ice-water condenser and then dewatered in a column of silica gel before it was sent to a micro gas chromatograph (Micro GC; Agilent) equipped with a thermal conductivity detector (TCD).

The CO conversion and selectivity to CH₄ are defined as follows:

$$X_{\text{CO}} (\%) = \frac{f_{\text{CO,in}} - f_{\text{CO,out}}}{f_{\text{CO,in}}} \times 100$$

and

$$S_{\text{CH}_4} (\%) = \frac{f_{\text{CH}_4,\text{out}}}{f_{\text{CO,in}} - f_{\text{CO,out}}} \times 100,$$

where X is the conversion of CO, S is the selectivity to CH₄ and f is the volumetric flow rate of CO or CH₄ which was determined from the GC-analyzed composition and the total gas flow rate estimated by taking the well-metered flux of N₂ as the internal standard.

The attrition of catalyst was evaluated with a few parameters defined according to the variation of particle size distribution (PSD) through an attrition test. These include the net change in the volume moment mean diameter and the increase in the fraction of fine particles (< 40 nm).^{14, 22} The volume moment mean diameter $d_{4,3}$ was calculated according to:

$$d_{4.3} = \frac{\sum d_i^4 N_i}{\sum d_i^3 N_i},$$

where d_i is the particle diameter and N_i is the number of particles with the size d_i . The net change in the volume moment mean diameter was expressed with the percentage against its initial value, as

$$\Delta Y (\%) = \left[\frac{Y(0) - Y(t)}{Y(0)} \right] \times 100,$$

where Y is the volume moment mean diameter ($d_{4.3}$). The increase in the fraction of fine particles below 40 μm was calculated by

$$\Delta F = F(t) - F(0),$$

where F represents the fraction of particles below 40 μm , and t is the time on stream ($t = 5$ h herein). The net change in volume moment mean diameter (ΔY) characterizes the average size change in an attrition test, and it not only decreases with increasing the amount of produced fines but is also affected by the breakup of agglomerates and large particles. The fraction of fines is a direct indication of the amount of fines generated from abrasion, and it is critical to the application of a catalyst for the fluidized bed reactor because it is determinative of the loss of the catalyst.

3. Results and discussion

3.1 Attrition evaluation

The measured attrition index shown in Table 1 reveals that the attrition resistance of the catalysts made by spray granulation followed an order of C-SS > C-AM > C-AS > C-CC in terms of the used binder. The catalyst using silica sol, especially acidic silica sol, as the binder had the higher attrition resistance than that using

alumina sol. For silica-binder catalysts, the attrition strength was improved through decreasing the pH value of the adopted binder (SS < AM < CC). The low pH value of the suspension made for spray granulation would enhance the mixing homogeneity and peptizing effect between the binder and catalyst precursor.²³ For comparison (benchmarking), Table 1 lists also the attrition index of a commercial γ -Al₂O₃ powder that is widely used as the support of many fluidized bed catalysts. One can see that the catalyst using SS as the binder was physically stronger than γ -Al₂O₃ powder, indicating its strong potential for use in fluidized bed.

It is believed that the particle attrition comes from both abrasion (removal of particle surface layers or corners) and fracture (fragmentation of particles).^{8, 24} Several studies have shown that there is an exponential relationship between particle size and particle strength resisting attrition.²⁴ In order to eliminate the effect of particle size on the measurement of attrition strength, all catalysts tested herein were sieved in advance. Corresponding to Table 1, Fig. 1 shows the PSDs of the catalysts made using different binders before and after the attrition test. All the tested catalysts presented a similar unimodal distribution of particle sizes in 40 to 125 μ m, and the median particle size with the cumulative size distribution fraction of 50% was about 63 μ m. After 5 h of attrition test, a bimodal distribution of particle size was obviously formed. As a result from fracture and abrasion, the average particle size decreased and the fraction of particles below 40 μ m increased, especially for the catalysts using AS and CC binders.

Table 1 lists also the major parameters calculated from the PSDs shown in Fig.1.

Corresponding to Fig. 1 (b), the small reduction in volume moment mean diameter ($\Delta Y = 9.0\%$) and slight increase in the fraction of fine particles (12.93%) show that abrasion played an important role in the attrition of C-SS. From Fig. 1 (a) and 1 (d) for C-AS and C-CC, one can see much high amount of fines (49.73% and 54.42%) accompanying with significant net changes in the volume moment mean diameter (34.82% and 37.54%). These indicate that such catalysts suffered not only severe abrasion but also fracture in attrition due to their weak mechanical strengths. Large particles broke into small parts, and this further enhanced the abrasion of particles to generate more fines. Meanwhile, a handful of particles above 125 μm can be seen in Fig. 1 (a) and 1 (d) for the attrited catalysts, possibly due to the agglomeration of small fragments in size measurement. Some fracture occurred besides abrasion in testing the attrition of C-AM to have the relatively large reduction in volume moment mean diameter (18.79%) and increase in fraction of fine particles (23.15%).

Figure 2 illustrates the morphologies of fresh and attrited catalysts. It is apparent that the silica-binder catalysts (2 (b1) - 2 (d1)) were basically microspheres with smooth external surfaces. However, the catalyst using AS as the binder had many irregular shapes such as teardrop or dumbbell caused by agglomeration, as shown in Fig. 2 (a1) with the dashed-line circle. With the attrition test, the catalyst using SS (2 (b2)) had little change in the particle size and morphology, further demonstrating the abrasion mechanism for its attrition. For C-AM, some small particles had rough surfaces because large particles broke into large fragments and small grains with angular corners. Then, the abrasion would make them smooth with the generation of a

big amount of fines. For C-AS and C-CC shown in Fig. 2 (a2) and 2 (d2), there were significant decreases in the number of large particles (above 60 μm) due to their disintegration into small fragments. Thus, high amounts of fine particles were observed to their severe attrition. No agglomerate was observed for C-AS after the attrition test (2 (a2)), implying that the breakage of agglomerates would occur role in this attrition test. All these observations from the SEM images verified the identified differences in attrition resistance characterized in terms of the attrition index, and it confirms also the accuracy of the results from PSDs shown above.

3.2 Attrition justification

Figure 3 shows the TEM images of catalyst precursor as well as calcined catalysts from spray granulation using different binders. The catalyst precursor (without binder) had the plate-like structure before (3 (a)) and after calcination (3 (b)). From Fig. 3 (c) to 3 (f) one can see that the large plate-like precursor particles in granulated catalyst using binders were covered by nanoscale binder particles. Binder particles on C-AS were more disordered and compact than that on silica-binder catalysts. The overlap of primary particles made it difficult to further analyze (distinguish) the inner structure of the catalysts.

From the TEM images of the granulated catalysts one can speculate that the formation of the catalyst granules followed the binding mechanism of “solid bridges”.²⁵ By adding the binder containing suspended colloidal particles to the precursor seriflux, liquid bridges are formed between the precursor particles, and colloidal particles in the liquid link together into a three-dimensional network. Via

spray drying, the colloidal solids concentrate by the diminishing liquid bridges, and the pressure due to surface tension of the liquid compacts the colloidal particles. After complete evaporation of the liquid the solid bridges are formed by deposition of colloidal particles. The large precursor particles are embedded in the continuous framework made of colloidal particles and bound together by the molecular forces in the remaining solid bridges.

The effects of binders on the textural characteristics of the granulated catalysts were studied by techniques of N₂ adsorption-desorption and high-pressure mercury displacement. Figure 4 shows resulting isotherms and estimated pore size distribution curves of fresh catalysts from spray granulation using different binders. According to the International Union of Pure and Applied Chemistry (IUPAC) classification,²⁶ all samples in Fig. 4 exhibited the type IV isotherms with a H3 hysteresis loop that is usually observed for slit-shaped mesopores resulting from aggregates of plate-like particles.

The BET surface areas, total pore volumes and average pore sizes of all catalysts are summarized in Table 2. Generally, the average pore size followed an order of C-AS > C-CC > C-AM > C-SS, in the reverse order for the BET surface area. After attrition test, the total pore volumes remained essentially the same for all catalysts, while their BET surface areas and average pore sizes slightly decreased. For the silica-binder catalysts, there was a trend that the attrition resistance increased with increasing the BET surface area and decreasing the average pore size. These are also the important parameters for the catalytic activity of the catalysts.

From Fig. 4 one can see that the pore size of C-AS and C-CC were concentrated at 16 nm, whereas that of C-SS and C-AM were around 10 nm. There was no large pore in the TEM images of calcined precursor (Fig. 3 (b)). Thus, the large pores such as above 20 nm may be piled pores from particle accumulation. Table 3 lists the pore volume measured by the N₂ physisorption and high-pressure mercury displacement techniques. The catalyst using AS had the higher volume of mesopores between 20 and 50 nm and less macropores (above 50 nm) in comparison with the silica-binder catalysts due to the more disorderly and closely aggregates of binder particles on the precursor in C-AS. For the catalysts using silica sol, the volume of pores (20-50 nm and above 50 nm) increased with increasing the pH value of the binder.

The preceding results assume that the volume of pores above 20 nm might have negative effects on the attrition strength of the catalysts made by spray granulation. In general, the attrition resistance sharply decreased with the increase in the volume of pores above 20 nm, especially for the catalysts using silica sol as the binder. This might be because that the granulated catalysts were composed of plate-like precursors and primary nanoscale binder particles. They aggregated and bound together by molecular forces²⁵ and formed slit-shaped pores. At extremely small distances among the catalyst particles such forces can become high, but they diminish quickly with increasing the distance.²⁵ Therefore, catalyst with more volume of large pores would easily fracture to suffer serious abrasion due to their weaker molecular forces. Comparatively, the weaker attrition resistance of C-AS depends not only on its higher volume of pores above 20 nm but also on the weaker strength of γ -Al₂O₃ skeleton.

Table 3 shows the average skeletal density from N₂ physisorption displacement and average particle density calculated with skeletal density and pore volume measured by mercury intrusion. For iron Fischer-Tropsch catalysts Zhao et al.¹⁶ found that the attrition strength increases with raising the particle density. Table 3 clarifies that for silica sol binder the catalyst attrition strength is directly proportional to the particle density of formed catalyst. The C-AS catalyst had the highest particle density, but its attrition strength was weak, possibly due to the weak attrition resistance of γ -Al₂O₃ skeleton.

3.3 More characterization

All catalysts made by spray granulation were further characterized through analyses using XRD and H₂-TPR to demonstrate the physiochemical features of active species and sites of the catalysts. Figure 5 shows the XRD patterns of the tested catalysts after calcination. The peaks at $2\theta = 37.2^\circ$, 45.6° and 66.7° can be considered as solid solutions (NiAl₂O₄, MgAl₂O₄ and Ni-Mg solid solution) and γ -Al₂O₃, while the peaks for NiO appeared at $2\theta = 37.2^\circ$, 43.2° and 62.8° corresponding to the (111), (200) and (220) planes, respectively. Nonetheless, it is difficult to distinguish the solid solutions and γ -Al₂O₃ due to overlapped reflections. Comparing with 20Ni and C-AS, the silica-binder catalysts had slightly decreased intensities for the peaks of solid solutions and γ -Al₂O₃ because of their lower Al₂O₃ contents. A broad peak between $2\theta = 18^\circ$ and 25° was observed in silica-binder catalysts to indicate the existence of amorphous SiO₂. The crystal sizes of NiO calculated using the Scherrer equation for the (200) plane were 7.78 nm for 20Ni, 7.42 nm for C-AS, 7.58 nm for C-SS, 9.24 nm

for C-AM and 7.88 nm for C-CC, respectively. All catalysts except for C-AM had the similar NiO crystal size as 20Ni, indicating binders of AS, SS and CC little influenced the crystal structure and NiO dispersity. For C-AM, some small NiO crystallites aggregated together and grew up during calcination, thus generating larger NiO crystals.

H₂-TPR was carried out to characterize the metal-support interaction. Figure 6 shows that there is mainly one H₂-consumption peak, occurring between 850 K and 1250 K, corresponding to the reduction of dispersed NiO that strongly interacts with Al₂O₃ or MgO.²⁷⁻³⁰ Hardly any free NiO that can be reduced at temperatures below 600 K could be identified, implying the well dispersion of NiO on all catalysts. Comparing with the interaction between NiO and γ -Al₂O₃, that between NiO and SiO₂ is weaker,^{31, 32} and NiO can hardly disperse on the surface of SiO₂ particles.³³ The counter diffusion of Ni²⁺ and Al³⁺ ions in 20Ni and C-AS were more active than in the silica-binder catalysts during calcination to cause their wider peaks of H₂ consumption in the TPR curves for 20Ni and C-AS.

The H₂ uptake in Table 3 was determined by H₂ chemisorption at 323 K to characterize the number of surface active sites. By assuming a stoichiometry ratio of H/Ni = 1 at the surface, the number of surface active sites was consistent with the measured H₂ uptake at 323 K. The amount of H₂-uptake followed an order of C-AS > C-SS > C-AM > C-CC, showing that the catalyst using AS as the binder had the largest number of surface active sites. In comparison with the catalyst without binder (21.5 $\mu\text{mol}\cdot\text{g}_{\text{cat}}^{-1}$) and with alumina sol (AS), the silica-binder catalysts had the less

surface active sites. As NiO can hardly disperse on the surface of SiO₂,³³ the added SiO₂ particles partially covered the NiO species in the precursor to decrease the surface active sites of silica-binder catalysts.

3.4 Activity evaluation

Figure 7 (a) shows the CO conversion and selectivity to CH₄ realized by all catalyst granules in a fluidized bed reactor operated at different temperatures under a pressure of 2.5 MPa and an SV of 120 NL·g⁻¹·h⁻¹. Take 623 K and 2.5 MPa as example, the minimum fluidization velocities (U_{mf}) of all catalysts calculated for the volume moment mean diameter are 1.415×10^{-3} m/s, 1.393×10^{-3} m/s, 1.302×10^{-3} m/s and 1.235×10^{-3} m/s for C-AS, C-SS, C-AM and C-CC, respectively. At this temperature the U/U_{mf} ratio was about 8, and it remained similar for all tested temperatures to ensure the good fluidization conditions. The CO conversion followed an order of C-AS > C-SS > C-AM \approx C-CC so that the catalyst C-AS using alumina sol as the binder had the highest catalytic activity to make its CO conversion over 90% at the tested temperatures. For the silica-binder catalysts, their CO conversions increased with increasing temperature until 780 K and then slightly decreased. At low reaction temperatures the syngas methanation over such catalysts may be subject to kinetic control, while above 780 K the equilibrium coefficient becomes low and the thermodynamic control tends to be predominant.³⁴ The C-AM and C-CC had almost the same CO conversion at all temperatures, while all catalysts had high selectivity of 83-90%. The preceding activity order was consistent with that of the surface active sites discussed above. Indeed, for methanation the dissociation of CO is the

rate-limiting step,³⁵ and more surface active sites can supply more active centers for the CO dissociation to raise the CO conversion.

The methanation carried out at high temperatures above 873 K can facilitate the recovery of exothermic heat from gaseous product. Figure 7 (b) shows the results from testing the stability of all catalysts in a fixed-bed reactor operated at 900 K, 2.5 MPa and an *SV* of 200 NL·g⁻¹·h⁻¹. Except for the slight decrease from 65% to 48% in the CO conversion over C-AM since 12 h of the test, the others had stable CO conversions and selectivity to CH₄ in the 20-h test. Further analysis shows that the realized selectivities of 84-86% for all the catalysts are very close to the theoretical selectivity of 87% calculated by assuming the thermodynamic control mechanism. Then, the little difference in the measured selectivities among different catalysts shown in Fig. 7(b) should be due to the experimental errors in molar concentration measurement and reaction temperature control.

Figure 8 shows the XRD patterns of the reduced (8 (a)) and spent (8 (b)) catalysts after a 20-h stability test under 2.5 MPa. The peaks for metallic Ni appeared at $2\theta = 44.3^\circ$, 51.7° and 76.1° corresponding to its (111), (200) and (220) planes, respectively. The crystal sizes of the metallic Ni calculated using the Scherrer equation for the (111) plane were 15.49 nm for C-AS, 15.20 nm for C-SS, 18.28 nm for C-AM and 16.27 nm for C-CC. There was no obvious change of the peaks for silica-binder catalysts before and after methanation. However, the spent C-AS catalyst (8 (b)) sharply increased the peak intensity of solid solutions or γ -Al₂O₃. Noting the good stability of the C-AS catalyst, this phenomenon might be caused by the growth

of the Al₂O₃ crystallite.

It was reported that carbon deposition often occurs on Ni catalysts,³⁶ and the CO disproportionation is a major way of carbon deposition for syngas methanation below 923 K. The total carbon amounts on the spent catalysts after the 20-h stability test at 2.5 MPa were analyzed using a CS-344 infrared analyzer. In turn the average carbon deposition rate was calculated, and Table 4 shows the results obtained. For the methanation under 2.5 MPa, the carbon deposition rate over the tested catalysts followed an order of C-CC > C-AM > C-SS > C-AS.

Figure 9 shows the TPO curves of the spent catalysts after the 20-h stability test at 2.5 MPa. There were at least three types of carbon deposited during methanation. The first peak is observed at about 570 K or below 660 K to indicate the most reactive carbon species C_α. The oxidation of the second type carbon C_β was between 660 K and 860 K, and the most inactive carbon C_γ is oxidized at temperatures above 860 K (e.g. 860-1030 K).³⁶⁻³⁸ The TPO curves in Fig. 9 are all fitted using the Gaussian-type functions, and the quantitative results are listed in Table 4.

The amount of each kind of carbon obviously varies with the catalyst used. On C-AS and C-SS, the C_α reached 48.9% and 42.7% respectively, nearly half of the total carbon deposited. Over C-AM and C-CC, only a small amount of C_α (21.2% and 25.3%) was identified. The carbon C_β was the main carbon species deposited on C-AM and C-CC, taking a proportion of 53.6% and 74.7%, respectively. The amount of C_γ deposited on C-AS, C-SS and C-AM were all about 25% of the total carbon deposited, whereas there was almost not C_γ on the C-CC catalyst. As reported,³⁶ the

inactive carbon C_γ is responsible for the deactivation of methanation catalyst through its encapsulation of catalyst surface and active sites. The large amount of C_γ deposited on C-AM due to the higher carbon deposition rate than C-AS and C-SS, might encapsulate the Ni crystallites of the catalyst and caused thus the decrease in the CO conversion in the stability test.

4. Conclusions

Spray granulation of catalyst precursor using different binders was employed to prepare attrition-resistant Ni-Mg/Al₂O₃ catalysts for fluidized bed methanation. Using the binders of alumina sol (AS, pH = 4.0), acidic silica sol (SS, pH = 3.0), alumina-modified silica sol (AM, pH = 8.7) and alkaline silica sol (CC, pH = 9.6) we prepared the catalysts C-AS, C-SS, C-AM and C-CC, respectively. Via air-jet attrition tests it was shown that the attrition strength followed an order of C-SS > C-AM > C-AS > C-CC, and C-SS had an attrition strength higher than the commercial γ -Al₂O₃ powder. The volume of pores above 20 nm was found to correlate well with the catalyst attrition strength. The higher the volume of pores above 20 nm, the easier the fracture of particles linked by small molecular forces to cause the lower attrition resistance. Using silica sol as the binder, the high particle density was also beneficial to improving the attrition strength.

Syngas methanation in a laboratory fluidized bed at 2.5 MPa and an SV of 120 NL·g⁻¹·h⁻¹ clarified an activity order of C-AS > C-SS > C-AM \approx C-CC at 623-923 K. Compared to silica-binder catalysts, the AS binder enabled highly dispersed metallic Ni and many surface active sites to facilitate methanation reactions. Via 20-h

continuous methanation tests at 900 K and 2.5 MPa it verified the stability of catalysts C-AS, C-SS and C-CC, whereas over C-AM the CO conversion decreased from 65% to 48%. The TPO curves for the spent catalysts demonstrated three types of carbon deposited on the catalysts. There was a high amount of inactive carbon (C_γ) on C-AM to cause the deactivation of the catalyst in the 20-h test by the encapsulation of surface Ni crystallites.

Hence, the binder for spray granulation is critical to the attrition strength and catalytic activity of the resulting catalyst granules. It was shown that the acidic silica sol likely led to high attrition resistance but relatively low catalytic activity especially at low methanation temperatures. The isothermal fluidized bed methanation allows high reaction efficiency and thus the use of catalysts with certainly low activity. This work showed that the catalyst C-SS is potentially suitable for the use in fluidized bed methanation due to its reasonably high attrition resistance as well as good catalytic activity even at 773 K. Nonetheless, further improvement is still needed for making commercial catalyst of fluidized bed methanation.

Acknowledgement

The authors are grateful to the financial support of National Natural Science Foundation of China (21161140329), International Science & Technology Cooperation Program of China (2013DFG60060), National Key Technology R&D Program (2012BAC03B05) and National High Technology Research and Development Program of China (863 Program, SS2015AA050502).

References

1. J. Kopyscinski, T. J. Schildhauer and S. M. A. Biollaz, *Fuel*, 2010, **89**, 1763-1783.
2. M. R. Rahimpour, M. R. Dehnavi, F. Allahgholipour, D. Iranshahi and S. M. Jokar, *Appl. Energy*, 2012, **99**, 496-512.
3. J. Kopyscinski, T. J. Schildhauer and S. M. A. Biollaz, *Chem. Eng. Sci.*, 2011, **66**, 924-934.
4. M. C. Seemann, T. J. Schildhauer and S. M. A. Biollaz, *Ind. Eng. Chem. Res.*, 2010, **49**, 7034-7038.
5. J. Kopyscinski, M. C. Seemann, R. Moergeli, S. M. A. Biollaz and T. J. Schildhauer, *Appl. Catal., A*, 2013, **462-463**, 150-156.
6. J. Liu, W. Shen, D. Cui, J. Yu, F. Su and G. Xu, *Catal. Commun.*, 2013, **38**, 35-39.
7. W. Z. Lu, L. H. Teng and W. D. Xiao, *Chem. Eng. Sci.*, 2004, **59**, 5455-5464.
8. C. R. Bemrose and J. Bridgwater, *Powder Technol.*, 1987, **49**, 97-126.
9. D. B. Bukur, X. Lang, D. Mukesh, W. H. Zimmerman, M. P. Rosynek and C. P. Li, *Ind. Eng. Chem. Res.*, 1990, **29**, 1588-1599.
10. D. B. Bukur, D. Mukesh and S. A. Patel, *Ind. Eng. Chem. Res.* 1990, **29**, 194-204.
11. M. E. Dry, in *Catalysis-Science and technology*, ed. J. R. Anderson and M. Boudart, Springer-Verlag, New York, 1981, vol. I , pp. 160-255.
12. K. Jothimurugesan, J. G. Goodwin, S. K. Gangwal and J. J. Spivey, *Catal. Today*, 2000, **58**, 335-344.
13. H. E. Bergna, in *Characterization and Catalyst Development: an interactive approach*, ed. S. A. Bradley, M. J. Gattuso and R. J. Bertolacini, American Chemical Society, Washington, DC, 1989, p. 55.
14. D. B. Bukur, W.-P. Ma, V. Carreto-Vazquez, L. Nowicki and A. A. Adeyiga, *Ind. Eng. Chem. Res.*, 2004, **43**, 16.
15. K. Jothimurugesan, J. J. Spivey, S. K. Gangwal and J. G. Goodwin, in *Natural Gas Conversion V*, ed. A. Parmaliana, D. Sanfilippo, F. Frusteri, A. Vaccari and F. Arena, 1998, vol. 119, pp. 215-220.
16. R. Zhao, J. G. Goodwin, K. Jothimurugesan, S. K. Gangwal and J. J. Spivey, *Ind. Eng. Chem. Res.*, 2001, **40**, 1065-1075.

17. Y. Yu, G.-Q. Jin, Y.-Y. Wang and X.-Y. Guo, *Fuel Process. Technol.*, 2011, **92**, 2293-2298.
18. J. R. Rostrup-Nielsen, K. Pedersen and J. Sehested, *Appl. Catal., A*, 2007, **330**, 134-138.
19. D. Liu, X. Y. Quek, W. N. E. Cheo, R. Lau, A. Borgna and Y. Yang, *J. Catal.*, 2009, **266**, 380-390.
20. J. Sehested, J. A. Gelten, I. N. Remediakis, H. Benggaard and J. K. Nørskov, *J. Catal.*, 2004, **223**, 432-443.
21. K. V. R. Chary, P. V. Ramana Rao and V. V. Rao, *Catal. Commun.*, 2008, **9**, 886-893.
22. R. Zhao, J. G. Goodwin and R. Oukaci, *Appl. Catal., A*, 1999, **189**, 99-116.
23. M. Kim, H.-J. Chae, T.-W. Kim, K.-E. Jeong, C.-U. Kim and S.-Y. Jeong, *J. Ind. Eng. Chem.*, 2011, **17**, 621-627.
24. British Materials Handling Board, *Particle Attrition, State-of-the Art Review*, Trans Tech Publications Inc., Zurich, Switzerland, 1987.
25. W. Piersch, in *Handbook of Powder Science & Technology*, Wiley, New York, 1991, pp. 24-30.
26. K. S. W. Sing, D. H. Everett, R. A. W. Haul, L. Moscou, R. A. Pierotti, J. Rouquerol and T. Siemieniewska, *Pure Appl. Chem.*, 1985, **57**, 603-619.
27. W. S. Dong, H. S. Roh, K. W. Jun, S. E. Park and Y. S. Oh, *Appl. Catal., A*, 2002, **226**, 63-72.
28. J. M. Rynkowski, T. Paryjczak and M. Lenik, *Appl. Catal., A*, 1993, **106**, 73-82.
29. C. Guimon, A. Auroux, E. Romero and A. Monzon, *Appl. Catal., A*, 2003, **251**, 199-214.
30. J. Zhang, H. Y. Xu, X. L. Jin, Q. J. Ge and W. Z. Li, *Appl. Catal., A*, 2005, **290**, 87-96.
31. P. Turlier, H. Praliaud, P. Moral, G. A. Martin and J. A. Dalmon, *Appl. Catal.*, 1985, **19**, 287-300.
32. M. Houalla, F. Delannay and B. Delmon, *J. Phys. Chem.*, 1981, **85**, 1704-1709.
33. L. F. Zhang, J. F. Lin and Y. Chen, *J. Chem. Soc. Faraday Trans.*, 1992, **88**,

2075-2078.

34. J. Liu, J. Yu, F. Su and G. Xu, *Catal. Sci. Technol.*, 2014, **4**, 472.
35. C. H. Bartholomew, *Catal. Rev.*, 1982, **24**, 67-112.
36. C. Mirodatos, H. Praliaud and M. Primet, *J. Catal.*, 1987, **107**, 275-287.
37. J. Guo, H. Lou and X. Zheng, *Carbon*, 2007, **45**, 1314-1321.
38. Z. L. Zhang and X. E. Verykios, *Catal. Today*, 1994, **21**, 589-595.

Table 1. Attrition results and NiO content of catalysts made by spray granulation using different binders.

Catalyst	NiO content (wt%) ^a	Attrition index (%)	$d_{4.3}$ (μm)		ΔY (%)	Fines fraction (vol%)
			fresh	attrited		
C-AS	22.52	7.64	63.00	41.07	34.82	49.73
C-SS	21.45	2.41	65.28	59.40	9.00	12.93
C-AM	21.51	3.97	66.85	54.29	18.79	23.15
C-CC	21.81	8.25	65.84	41.12	37.54	54.42
$\gamma\text{-Al}_2\text{O}_3$	-	2.95	72.30	62.43	15.81	19.52
20Ni	21.19	-	-	-	-	-

^a The NiO content was determined by XRF.

Table 2. Characterization of catalysts from spray granulation using N₂ physisorption.

Catalyst	BET surface area (m ² ·g ⁻¹) ^a		Pore volume (cm ³ ·g ⁻¹) ^b		Average pore size (nm) ^c	
	fresh	attrited	fresh	attrited	fresh	attrited
C-AS	104	99	0.47	0.50	16.17	15.55
C-SS	124	119	0.46	0.42	13.19	12.40
C-AM	118	115	0.46	0.43	13.71	13.54
C-CC	115	113	0.48	0.45	15.73	15.63

^a Calculated with the BET equation.

^b Referring to the BJH desorption pore volume.

^c Referring to the BJH desorption average pore size (4×total pore volume/ surface area).

Table 3. Porosity, density and H₂ uptake of catalysts from spray granulation.

Catalyst	Pore volume (20 ~50 nm) (cm ³ ·g ⁻¹) ^a	Pore volume (macropore) (cm ³ ·g ⁻¹) ^b	Skeletal density (g·cm ⁻³) ^c	Particle density (g·cm ⁻³) ^d	H ₂ uptake (μmol·g _{cat} ⁻¹) ^e
C-AS	0.226	0.0331	3.38	1.26	20.9
C-SS	0.115	0.0319	2.86	1.24	10.1
C-AM	0.155	0.0408	2.89	1.16	6.6
C-CC	0.183	0.0501	2.91	1.10	6.2

^a Measured by N₂ physisorption, error = ±5% of the value measured.

^b Measured by High-pressure mercury porosimetry, error = ±10% of the value measured.

^c Determined by N₂ physisorption displacement, error = ±5% of the value measured.

^d Calculated using the skeletal density and total pore volume.

^e Determined by H₂ chemisorption.

Table 4. Average carbon deposition rate and TPO quantitative data of spent catalysts.

Catalyst	C deposition rate ($\times 10^{-2}$ wt% \cdot h $^{-1}$) ^a	T _m (K) ^b			Fraction of total area (%)		
		α	β	γ	α	β	γ
C-AS	2.0	583	720	890	48.9	31.5	19.6
C-SS	3.0	567	823	914	42.7	30.6	26.7
C-AM	4.2	561	812	931	21.2	53.6	25.2
C-CC	7.2	567	785	-	25.3	74.7	-

^a The average carbon deposition rate is the ratio of total deposited carbon over reaction time, and the total carbon amount was determined by a CS-344 infrared analyzer.

^b T_m indicates the temperature at the center of every carbon peak in Fig. 9.

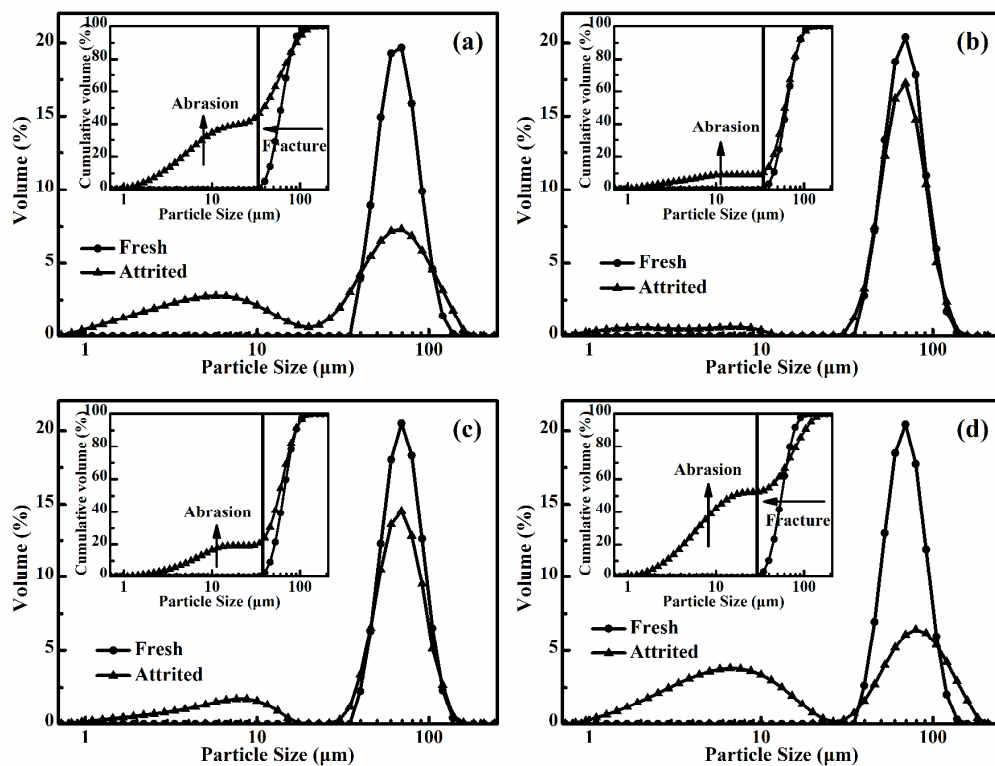


Fig. 1 Particle size distributions of catalysts from spray granulation before and after attrition test: (a) C-AS, (b) C-SS, (c) C-AM and (d) C-CC.

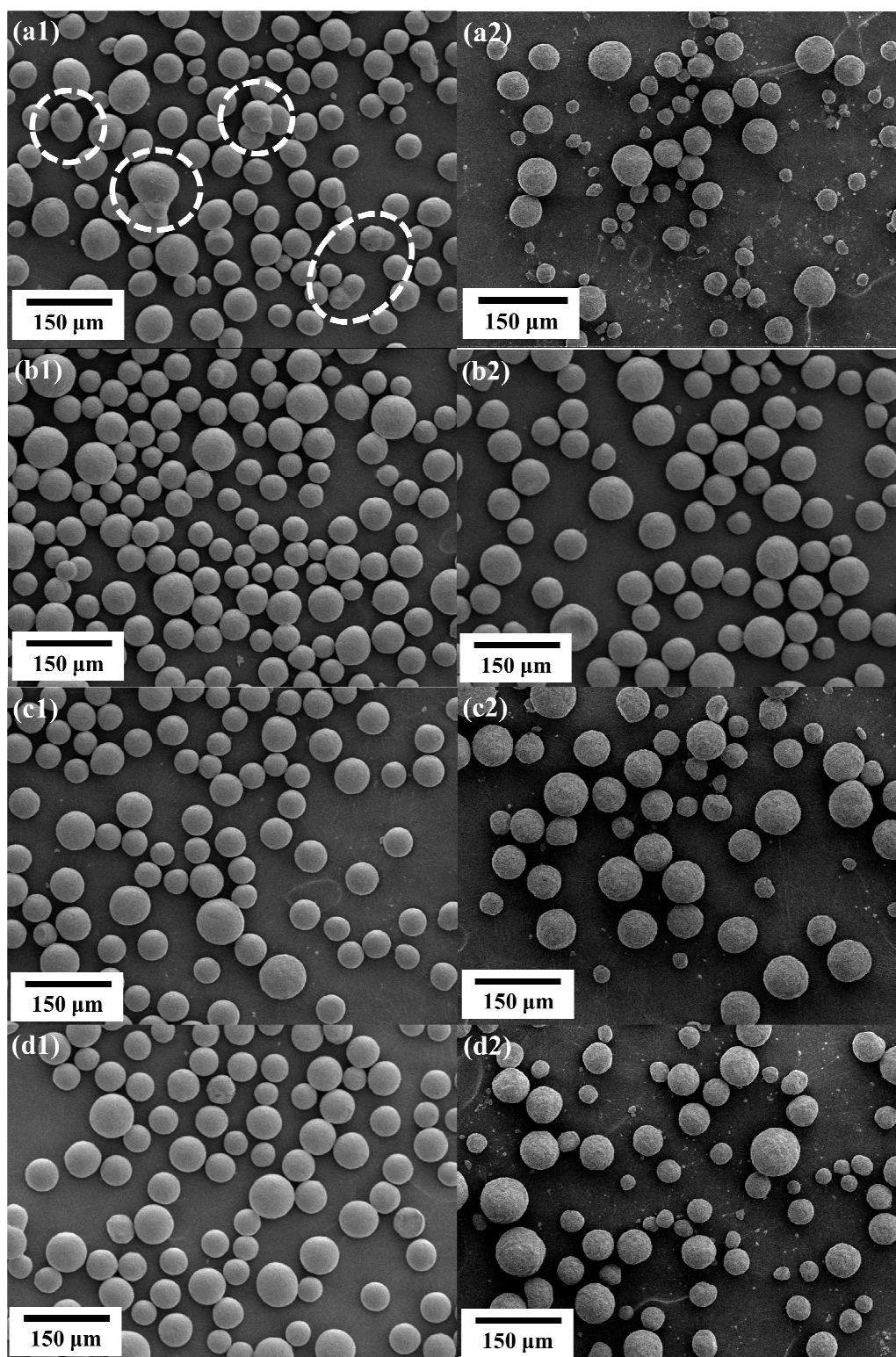


Fig. 2 Morphologies of catalysts from spray granulation before (left) and after (right) attrition test : (a) C-AS, (b) C-SS, (c) C-AM and (d) C-CC.

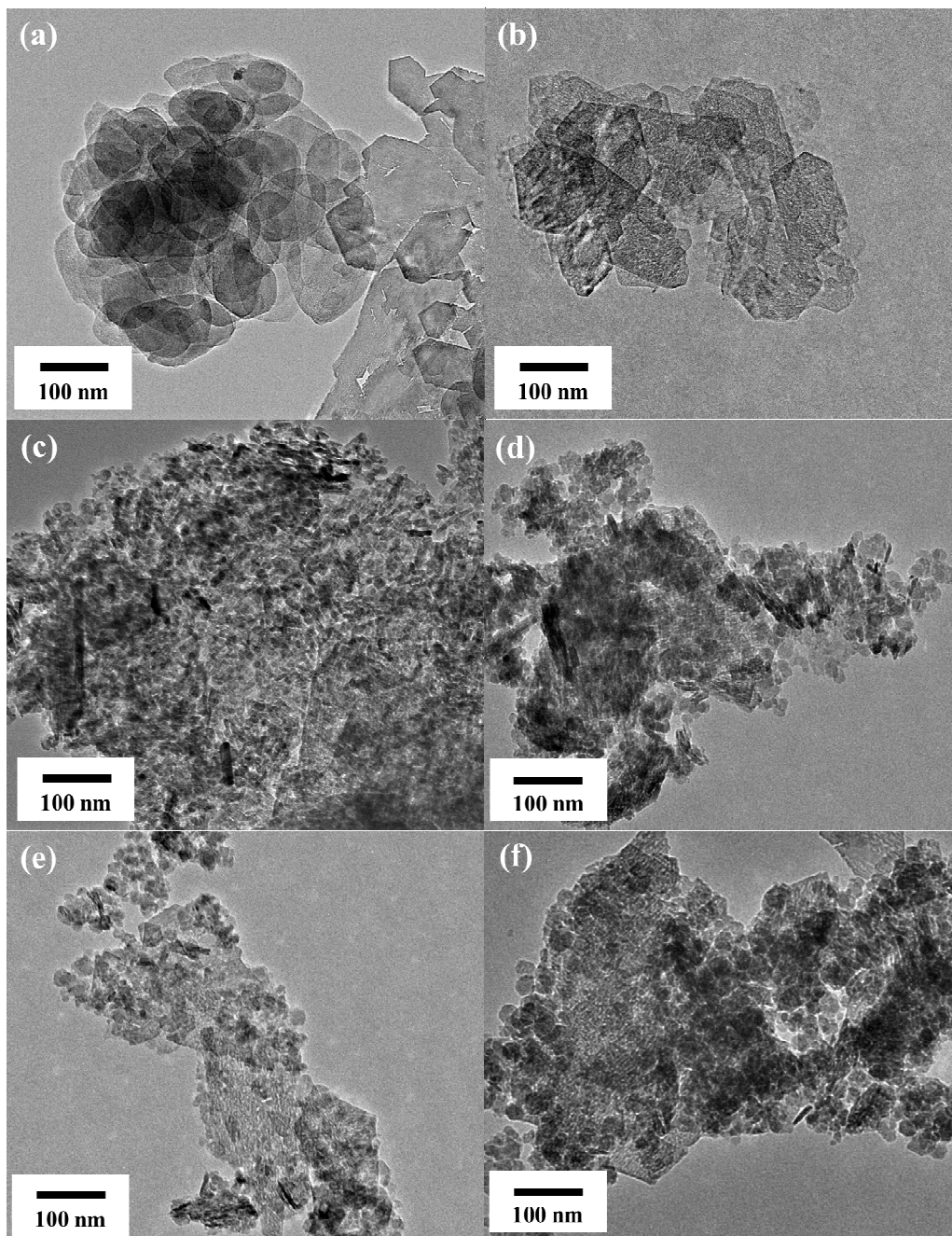


Fig. 3 TEM images of catalyst precursors (a) before and (b) after calcination, and of the catalysts from spray granulation after calcination for (c) C-AS, (d) C-SS, (e) C-AM and (f) C-CC.

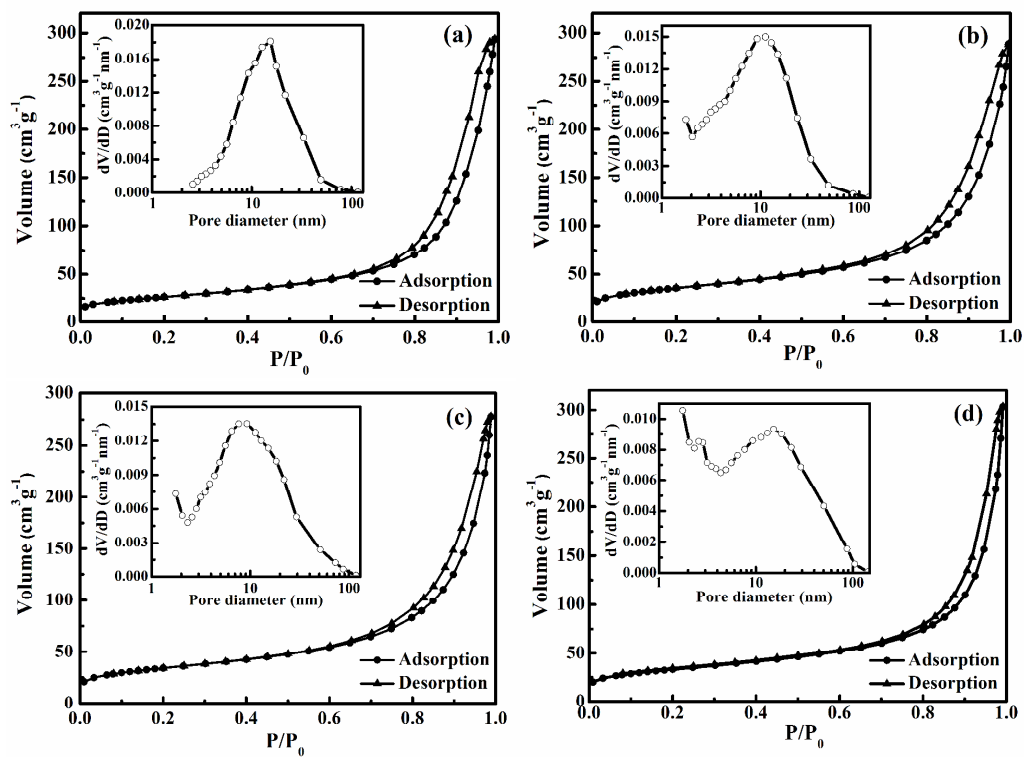


Fig. 4 N_2 adsorption-desorption isotherms and pore size distribution curves of the fresh catalysts from spray granulation using different binders: (a) C-AS, (b) C-SS, (c) C-AM and (d) C-CC.

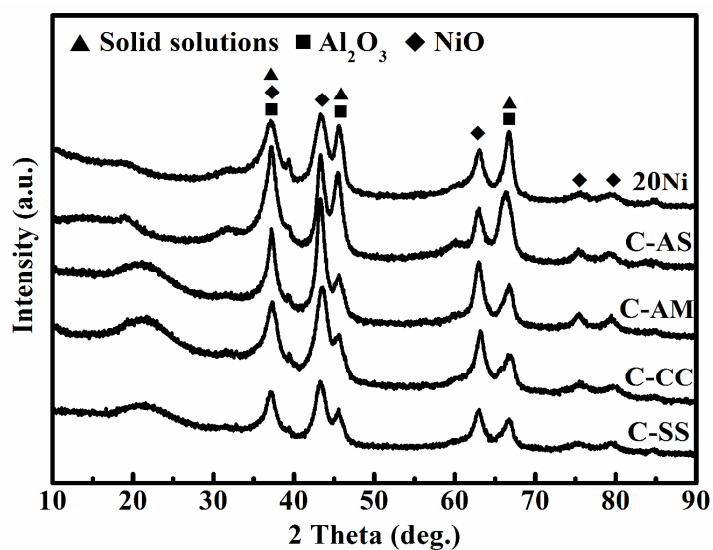


Fig. 5 XRD patterns of tested catalysts after calcination (solid solutions include NiAl₂O₄, MgAl₂O₄ and Ni-Mg solid solution).

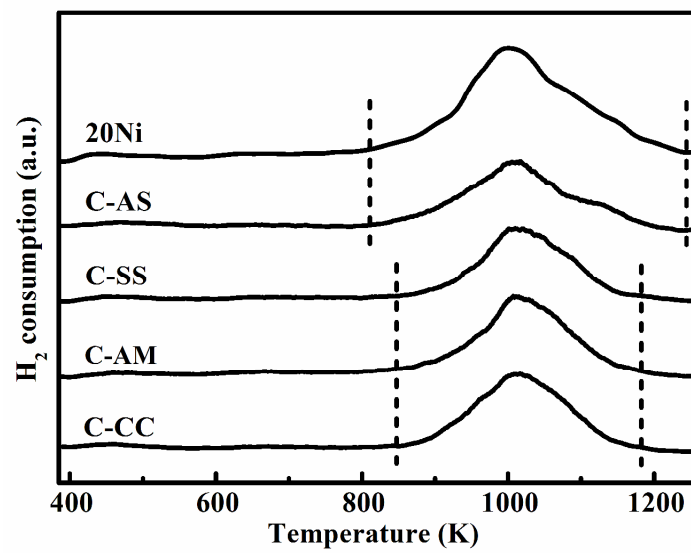


Fig. 6 H₂-TPR curves of spray-granulated catalysts in 10% H₂/Ar under a heating rate of 5 K/min.

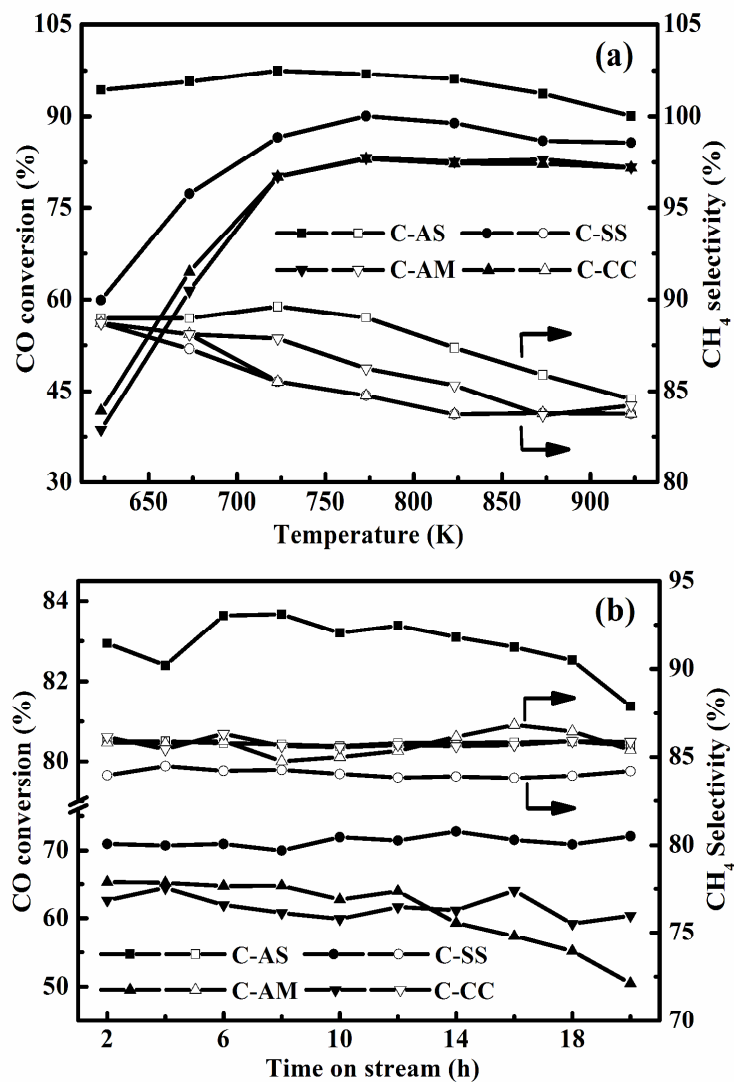


Fig. 7 CO conversion and selectivity to CH₄ varying with (a) reaction temperature ($SV = 120 \text{ NL}\cdot\text{g}^{-1}\cdot\text{h}^{-1}$) and (b) reaction time ($T = 900 \text{ K}$, $SV = 200 \text{ NL}\cdot\text{g}^{-1}\cdot\text{h}^{-1}$) under 2.5 MPa over granulated catalysts using different binders.

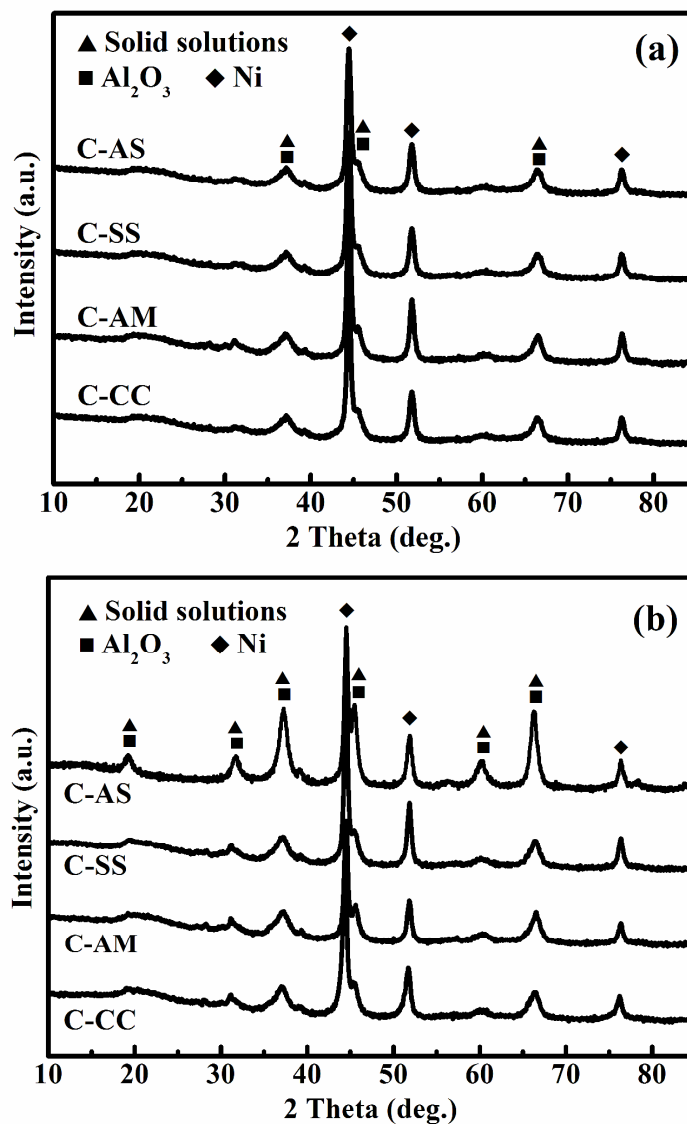


Fig. 8 XRD patterns of (a) reduced by raising temperature to 1273 K at $5\text{ K}\cdot\text{min}^{-1}$ in N_2 -base 10 vol% H_2 gas and (b) spent catalysts after 20-h stability test at 900 K and 2.5 MPa, where solid solutions include NiAl_2O_4 , MgAl_2O_4 and Ni-Mg solid solution.

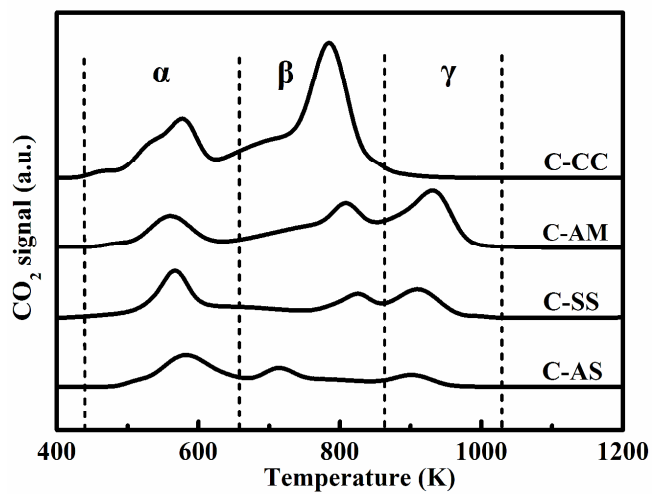


Fig. 9 TPO curves of spent catalysts after 20-h stability test at 900 K and 2.5 MPa.

Investigating the granular Ni-Mg/Al₂O₃ prepared by spray granulation of catalyst precursor using different binders has demonstrated that the used binder is critical to the attrition strength and catalytic activity for syngas methanation of the resulting catalysts, and it was shown that the catalyst using the binder of acidic silica sol (SS) is potentially suitable for the use in fluidized bed methanation due to its reasonably high attrition resistance (attrition index: 2.41%, better than γ -Al₂O₃) and good catalytic activity even at 773 K (only next to C-AS).

